2D Materials

PAPER

Interlayer and interfacial stress transfer in hBN nanosheets

Weimiao Wang, Zheling Li ⬤, Alex J Marsden ⬤, Mark A Bissett ⬤ and Robert J Young* ⬤

National Graphene Institute and Department of Materials, University of Manchester, Manchester M13 9PL, United Kingdom
* Author to whom any correspondence should be addressed.

E-mail: robert.young@manchester.ac.uk

Abstract

Stress transfer has been investigated for exfoliated hexagonal boron nitride (hBN) nanosheets (BNNSs) through the use of Raman spectroscopy. Single BNNSs of different thicknesses of up to 100 nm (300 layers) were deposited upon a poly(methyl methacrylate) (PMMA) substrate and deformed in unixial tension. The Raman spectra from the BNNSs were relatively weak compared to graphene, but the in-plane E_{2g} Raman mode (the G band) could be distinguished from the spectrum of the PMMA substrate. It was found that G band down-shifted during tensile deformation and that the rate of band shift per unit strain decreased as the thickness of the BNNSs increased, as is found for multi-layer graphene. The efficiency of internal stress transfer between the different hBN layers was found to be of the order of 99% compared to 60%–80% for graphene, as a result of the stronger bonding between the hBN layers in the BNNSs. The reduction in bandshift rate can be related to the effective Young's modulus of the 2D material in a nanocomposites and the findings show that it would be expected that even 100 layer BNNSs should have a Young's modulus of more than half that of hBN monolayer. Interfacial stress transfer between a single hBN nanosheet and the PMMA substrate has been evaluated using shear lag theory. It is found that the interfacial shear stress between the BNNS and the substrate is of the order of 10 MPa, a factor of around 4 higher than that for a graphene monolayer. These findings imply that BNNSs should give better mechanical reinforcement than graphene in polymer-based nanocomposites as a result of good internal interlayer stress transfer within the nanosheets and better interfacial stress transfer to the polymer matrix.

1. Introduction

Since the successful exfoliation of graphene [1], ultrathin two-dimensional (2D) materials with excellent but diverse mechanical, optical, thermal and electronic properties [2, 3], have attracted worldwide attention. Just a few months after the isolation of graphene, there was the first report [4] of successfully exfoliating nanometre-thick 2D hexagonal boron nitride (hBN) nanosheets (BNNSs). Compared with their carbon analogue, BNNSs exhibit superior oxidation resistance [5] and chemical and thermal stability [6, 7]. In addition, the reduced electron-delocalization in the B–N π bonds leads to a large ~6 eV band gap [8], making BNNSs both electrically insulating and optically transparent [9]. The exceptional thermal and electrical properties of BNNSs

suggest that they have potential applications in various fields, such as nanofillers for polymer nanocomposites [10, 11] and researchers on BNNS/polymer composites have concentrated principally upon the modification of the thermal conductivity and insulating properties by the addition of BNNNs [12–16]. Mechanical reinforcement has, in contrast, been less well studied. Pioneering work upon the mechanical reinforcement of polymers with BNNSs was carried out in 2009 [17] in which BNNSs were exfoliated using a liquid exfoliation-centrifugation technique. The as-prepared BNNSs were added into poly(methyl methacrylate) (PMMA) and an improvement in the Young's modulus and increase of tensile strength were achieved. Reinforcement of poly(vinyl alcohol) by BNNSs was then reported by Khan *et al* [18] who also found improvements in mechanical properties. Other

studies have reported increases in Young's modulus and tensile strength upon the addition of BNNS for both polycarbonate [19] and polyethylene [20].

Although BNNSs have been investigated for mechanical reinforcement for a number of years, it is only recently that their fundamental mechanical properties have been studied systematically [21]. Theoretical calculations predicted a high Young's modulus and fracture strength of monolayer hBN to be in the ranges 0.72–0.98 TPa and 68–215 GPa, respectively [22–26], values close to the experimental ones for monolayer (1L) graphene (∼1 TPa and 70–130 GPa) [27]. Earlier, Song *et al* [22] has reported a modulus of 0.33 ± 0.02 TPa and fracture strength of 26.3 GPa for their chemical-vapour-deposition (CVD)-grown bilayer (2L) BNNSs, much lower than the predicted values. Their poor mechanical properties were attributed to the presence of defects and grain boundaries [28, 29]. Another study [30], however, reported a higher measured Young's modulus of 1.16 ± 0.1 TPa for a CVD-grown BNNS with ∼45 layers. Considering the variable quality of CVD-grown BNNSs and the consequences for their intrinsic strength, Falin *et al* [21] undertook the first systematic measurements upon mechanically-exfoliated BNNSs with different numbers of layers. By using atomic force microscope (AFM) nanoindentation [27], the Young's modulus of exfoliated single-crystalline 1L, 2L, 3L hBN was measured to be 0.87 ± 0.07 TPa, 0.88 ± 0.06 TPa, 0.81 ± 0.04 TPa, with breaking strengths of from one to three layers is 70.5 ± 5.5, 68.0 ± 6.8, 76.9 ± 2.3 GPa respectively. Such impressive mechanical properties make BNNSs amongst the strongest insulators. More importantly, this work also revealed that interlayer bonding within BNNSs appears to be much stronger than in the case of multi-layer graphene. The Young's modulus and strength of graphene decrease rapidly with increasing thickness. Both properties remain almost constant for BNNSs when the number of layers increases from one to nine. Hence multilayer BNNSs are predicted to show different mechanical behaviour to graphene in nanocomposites as a result of the strict AA' stacking order and strong 'lip-lip' interaction between adjacent layers [31–33]. On the other hand, the level of layer–layer stress transfer efficiency of BNNSs during deformation is, to our knowledge, yet to be quantified.

As summarized in a recent review [34], previous work upon graphene-reinforced nanocomposites has shown that many aspects of 2D materials affect their ability to reinforce nanocomposites. We have shown that Raman spectroscopy can be employed to investigate the dispersion [35, 36], orientation [37, 38], interface with polymer matrices [39], flake size and layer–layer interactions [40, 41] etc for graphene-related materials and evaluate their effects on the mechanical reinforcement of nanocomposites. There are a few reports of using Raman-spectroscopy to study the mechanical behaviour of BNNSs. Cai *et al* [42] heated then cooled exfoliated different BNNSs on a SiO_2/Si wafer and found different degrees of blue shift for the in-plane E_{2g} Raman mode (normally denoted as the 'G band') of BNNSs for different sheet thicknesses. Androulidakis *et al* [43] reported the first measurement of uniaxial strain-induced Raman band shifts for 2L–4L BNNSs. They exfoliated the BNNSs from a bulk BN single crystal and transferred them on a SU-8/PMMA substrate. The polymer substrate was then stretched uniaxially. Although the Raman signal of BNNSs on the polymer substrate is very weak due to the wide band gap of hBN, both a shift to lower frequency and band splitting with increasing tensile strain were observed for the G band of the BNNSs at ∼1368 cm^{-1}. It was found that the shift of G band frequency generally showed a linear relationship with applied strain at low strain but become irregular when the strain was higher than ∼0.3%, suggesting a relatively poor interfacial interaction between the BNNSs and the polymer substrate. In addition, the G band shift rates was almost constant when the number of layers increased from two to four, again demonstrating strong layer–layer bonding within the BNNSs.

Previous work on exfoliated monolayer graphene has demonstrated that the effective Young's modulus (E_{eff}) of 2D materials in nanocomposites is controlled by both their intrinsic modulus and the layer–layer stress transfer efficiency of the 2D materials [41]. Additionally it was shown that the lateral dimensions of a 2D material control stress transfer between the material and the polymer matrix thereby affecting their ability to reinforce polymers [40]. In this present study we have employed Raman spectroscopy to investigate the effect of both the BNNS thickness and lateral dimensions upon stress transfer from a polymer substrate.

2. Experimental

2.1. Materials

For mechanical exfoliation, large commercial hBN single crystals were purchased from HQ Graphene and used as received. The single crystals were exfoliated mechanically and the flakes transferred using the standard tape cleavage technique [44]. The BNNSs were exfoliated using blue adhesive tape (Nitto Denko Corporation) and deposited directly on the centre of a rectangular PMMA beam with no top coat applied, as illustrated in figure S1 (available online at stacks.iop.org/2DM/8/035058/mmedia) in the supplementary information.

2.2. Characterization

The BNNSs on the PMMA beams were identified and characterized using the Zeiss optical microscope on a Horiba LabRAM Evolution HR spectrometer with a 50× lens. The thickness of the BNNSs on the beams was measured using a Nanowizard AFM (JPK Instruments) operated in the QI mode.

Figure 1. (a) Optical micrograph and (b), (c) AFM images of three marked spots on the two BNNS flakes. (d)–(f) The height profiles correspond to the three solid lines in (b), (c). (g) Raman spectra of the three marked spots on the BNNSs. (h)–(j) Raman spectra of the three marked spots on the BNNSs before and after up to 0.24% tensile strain was applied. (k) The position of Raman G band as a function of tensile strain for the three marked spots on the BNNSs.

2.3. *In situ* Raman deformation studies

The Horiba LabRAM Evolution HR spectrometer equipped with 488 nm sapphire laser was used for the analysis of the mechanically-exfoliated BNNSs. The *in-situ* Raman deformation analysis was conducted by inserting the BNNS-loaded PMMA beams into a four-point-bending rig fixed on the Raman microscope stage. A resistance strain gauge was used on the PMMA beam surface to monitor the strain applied on the PMMA substrate. The beams were deformed up to 0.4% strain in ~0.04% intervals and Raman spectra were collected and peak fitted at each strain level. The exposure time for each Raman scan was 20 s with a power output ~1.3 mW and a laser spot size of ~2 μm using a 50× objective lens. The most prominent Raman band of hBN is the E_{2g} mode which originates from in-plane atomic displacement and is equivalent to the G band of graphene [45]. Raman line mapping was undertaken using a 100× objective lens.

3. Results and discussion

3.1. Strain-induced Raman band shifts

Figure 1 gives the result of *in-situ* Raman deformation studies of two BNNSs transferred onto a PMMA beam. An incremental strain up to 0.4% was applied parallel to the long axis of the BNNSs as shown in figure 1(a). The Raman spectra obtained at three different spots (marked and denoted as spots 1–3 in figure 1(a)) were recorded simultaneously at each strain level. As shown in figures 1(d)–(f). The measured thickness of the BNNSs at each spot 1–3 is 10.0, 8.8 and 20.0 nm, respectively. The corresponding spectra obtained under similar conditions at each

spot are shown in figure 1(g) and it can be seen that spot 3, from the thickest BNNS, exhibits the strongest hBN G band.

It can be seen in figures 1(h)–(j) that the G bands of the Raman spectra collected at the three spots all shifted to lower wavenumber under the application of tensile strain. Figure 1(k) shows that there was a linear downshift to lower frequency up to ~0.2% strain and the derived shift rates in the low strain region for spots 1–3 are -8.1 ± 1.6 cm^{-1}/%, -9.4 ± 0.6 cm^{-1}/%, -7.7 ± 0.9 cm^{-1}/%, respectively. These measurements show that the shift rate drops slightly as the thickness of the BNNSs increases from 8.8 to 20 nm. This suggests that, unlike few-layer graphene, where there is a significant decrease in shift rate (per % stain) with increasing flake thickness due to easy inter-layer sliding [41], the layer–layer interaction inside the BNNSs is relatively strong [21, 43]. These rates of G-band shift are similar to those reported in an earlier study upon the deformation of exfoliated BNNSs on a PMMA substrate [43]. We sometimes observed some broadening G-band as shown in figure S2 in the supplementary information but did not, however, see any band splitting, possibly as the result of the low levels of applied strain used in our study.

It can also be observed in figure 1(k) that the downshift of the three spots reduces when the strain exceeds ~0.2%, indicating possible BNNS slippage on the substrate at a relatively low strain. This implies that surface modification of pristine BNNSs may be necessary to ensure their interfacial adhesion with a polymer matrix in order to realize good reinforcement, as reported in a recent study upon hBN nanotubes in nanocomposites [46].
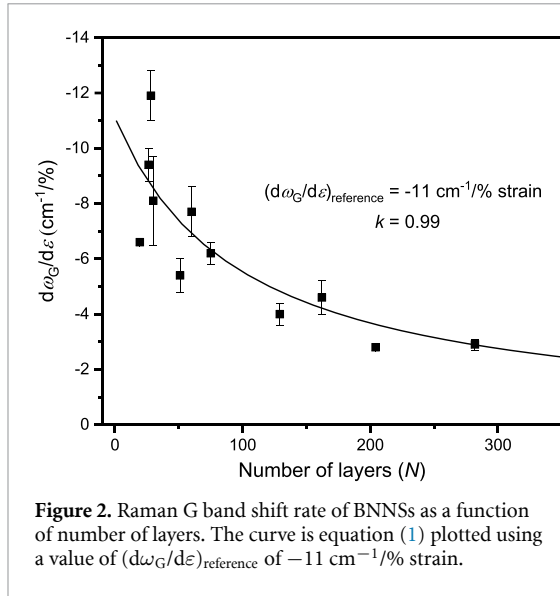
Figure 2. Raman G band shift rate of BNNSs as a function of number of layers. The curve is equation (1) plotted using a value of $(d\omega_G/d\varepsilon)_{reference}$ of -11 cm^{-1}/% strain.

3.2. Interlayer stress transfer

To investigate further the effect of the number of layers, we exfoliated more BNNSs and studied their Raman G band shift rates as a function of thickness (see table S1 in the supplementary information). The highest downshift rate (-11.9 cm^{-1}/%) was found for a hBN nanosheet of 9.4 nm thickness (28 layers, assuming an individual layer thickness of 0.333 nm [47]), and the shift rate was found to gradually decrease with an increasing number of layers eventually dropping to ~ -2 cm^{-1}/% when the thickness increased to $\sim$100 nm (300 layers). The data in table S1 in the supplementary information are plotted in figure 2. They are fitted to the equation for the effect of the number of layers upon the Raman band shift rate ($d\omega/d\varepsilon$) derived in a previous study upon few-layer graphene [41]:

$$(d\omega_G/d\varepsilon) = \frac{(d\omega_G/d\varepsilon)_{reference}}{[N - k(N-1)]} \qquad (1)$$

where N is the number of layers and k is the interlayer transfer efficiency. The parameter $(d\omega_G/d\varepsilon)_{reference}$ is the reference G band shift rate for monolayer hBN ($N = 1$). Fitting equation (1) to the data in figure 2 gives a value of -11 cm^{-1}/% for $(d\omega_G/d\varepsilon)_{reference}$ and an interlayer transfer efficiency k of $\sim$0.99 (i.e. 99% efficient). This is much higher than the stress transfer efficiency determined for few-layer graphene (0.6–0.8) [41]. Most of the measurements in figure 2 were taken during deformation from a region approximately the middle of the BNNS. It will be shown below that the strain will vary with position on the flake which might account for some of the scatter of the data in figure 2.

The evaluation of the parameter k can also be used to predict the dependence of the Young's modulus of a 2D material in a nanocomposite upon the number of layers, N. In the case of 2D materials laid on the

surface of the polymer beam without any top coating, such as in this present study, the effective modulus E_{eff} is given by [41]:

$$E_{eff} = \frac{E_{2D\ material}}{[N - k(N-1)]} \qquad (2)$$

where $E_{2D\ material}$ is the Young's modulus of the 2D material monolayer. A value of $k = 0.99$ means that E_{eff} will only fall to half of the monolayer value for 100-layer BNNS ($N = 100$). This can be contrasted with the behaviour of multilayer graphene for which k is in the range of 0.6–0.8. Its modulus falls rapidly to half the monolayer value for $N = 5$ when $k \sim 0.7$. Hence it appears that it is less important to achieve a high degree of exfoliation to very thin nanosheets, when using hBN in nanocomposites, than in the case of graphite and graphene.

3.3. Grüneisen parameter

It is also possible to determine the Grüneisen parameter for the BNNSs using the relationship:

$$\gamma_G = \frac{\Delta\omega_G}{\omega_G^0 (1 - \nu)\varepsilon}. \qquad (3)$$

The Raman frequency of the G band (ω_G^0) is 1366 cm^{-1} and the Poissons ratio of the PMMA matrix $\nu = 0.35$ [43, 48]. Setting $\Delta\omega_G/\varepsilon = (d\omega_G/d\varepsilon)_{reference}$, the value of the Grüneisen parameter γ_G of the BNNS is calculated to be 1.24. This value is close to the value of $\gamma_G = 1.34 \pm 0.72$ we found for hBN nanotubes in our previous study [46] and the value of $\sim$1.04 reported by Androulidakis *et al* [43] for BNNSs with >10 layers.

3.4. Strain mapping

Our previous work on 1L graphene [40] has demonstrated that it is possible to monitor stress transfer from a substrate to the flake of a 2D material by mapping the strain along the flake. Figures 3(a) and (b) shows a hBN nanosheet of 11 μm length and 17 nm (figure 1(c)) in thickness deformed in tension parallel to its axis. To improve the spatial resolution of the linear strain mapping, an objective lens with the highest resolution ($\times$100) was used to minimize the laser spot size to $\sim$1.5 μm. Thus an intense G band for the BN nanosheet can be seen in figure 3(d). Figure 3(e) shows the Raman spectra obtained from the middle of the nanosheet (marked by a black square in figure 3(b)) before and after 0.2% strain was applied. It can be seen that the G band clearly shifts to lower frequency and broadens after deformation. The broadening a result of band splitting [43] but the band has for simplicity been fitted to a single peak in this present study. As shown in figure 3(f), there is a linear red shift of the G band with stepwise straining up to 0.15%. The shift stops at 0.2% strain and eventually became irregular when a higher tensile strain was applied.
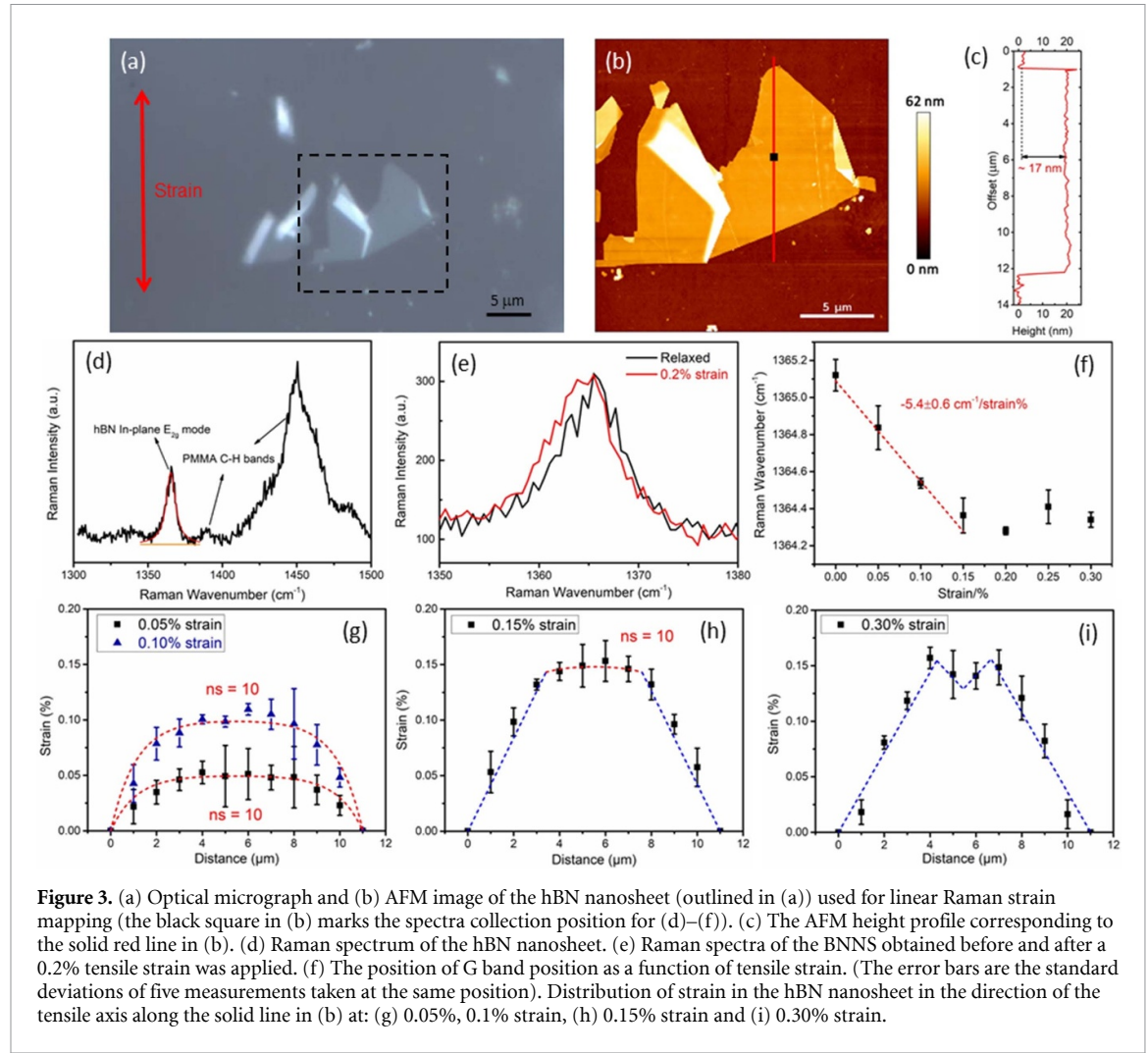
Figure 3. (a) Optical micrograph and (b) AFM image of the hBN nanosheet (outlined in (a)) used for linear Raman strain mapping (the black square in (b) marks the spectra collection position for (d)–(f)). (c) The AFM height profile corresponding to the solid red line in (b). (d) Raman spectrum of the hBN nanosheet. (e) Raman spectra of the BNNS obtained before and after a 0.2% tensile strain was applied. (f) The position of G band position as a function of tensile strain. (The error bars are the standard deviations of five measurements taken at the same position). Distribution of strain in the hBN nanosheet in the direction of the tensile axis along the solid line in (b) at: (g) 0.05%, 0.1% strain, (h) 0.15% strain and (i) 0.30% strain.

The Raman G band position was monitored along the solid line in figure 3(b) in 1 μm steps. Figure 3(g) shows the variation of axial strain across the BNNSs flake when a low strain ($\leqslant$0.1%) was applied to PMMA substrate. It can be seen that the strain builds up from the two edges and becomes constant along the middle of the nanosheet where the strain in the flake equals to the applied matrix strain. This is analogous to what we observed for the strain distribution of a polymer-sandwiched graphene monolayer under relatively low strain (<0.4%) [40] for which there was good bonding between 2D material and polymer matrix. This behaviour can be analysed by the well-established shear-lag theory [49, 50] where it is assumed that the elastic stress is transferred from the matrix to the reinforcement through a shear stress at 2D material/polymer interface. The variation of strain in the BNNS, $\varepsilon_{\mathrm{BNNS}}$, is given as [34]:

$$\varepsilon_{\mathrm{BNNS}} = \varepsilon_{\mathrm{m}} \left[1 - \frac{\cosh\left(ns\frac{x}{l}\right)}{\cosh(ns/2)} \right] \quad (4)$$

where,

$$n = \sqrt{\frac{2G_{\mathrm{m}}}{E_{\mathrm{BNNS}}} \left(\frac{t}{T}\right)} \quad (5)$$

and ε_{m} is the applied matrix strain, s is the aspect ratio of the BNNS, x represents the position in the flake, l is the length of the flake, G_{m} is the matrix shear modulus, E_{BNNS} is the Young's modulus of the 2D material, t is the thickness of the BNNS and T is the thickness of polymer matrix. The parameter n has been widely accepted as a parameter for evaluating the interfacial stress transfer efficiency. The dashed line in figure 3(g) is a reasonable fit of equation (4) to the Raman mapping results using $ns \approx 10$. The aspect ratio for the hBN nanosheet in figure 3 is $s = 10\,\mu$m/17 nm ≈ 590. Since for this BNNS, $ns = 10$ and so $n = 0.017$. This value of n is some 30$\times$ larger that the value of $n = 6 \times 10^{-4}$ determined for a sandwiched graphene monolayer on a polymer substrate [40]. The higher value of n implies that better stress transfer can be expected between BNNSs and a polymer matrix than for graphene, presumably a result of the more polar nature of the bonding in hBN.

It can be seen in figure 3(g) that the strain rises to about 90% of the plateau value over about 3 μm from the edge, suggesting the critical length l_{c} of the few-layer BNNS reinforcement of the order of 6 μm. The value of critical length determined for monolayer graphene using a similar approach is ~3 μm

[40], but it should be noted that the BNNS flake in figure 3 is 17 nm thick. Hence the critical aspect ratio, s_c, for this 50-layer BNNS is ∼350 compared with a value of around 10^4 (≈3 μm/0.35 nm) for monolayer graphene. This is further indication that BNNSs should give good reinforcement in nanocomposites at lower levels of exfoliation than for graphene. The importance of the aspect ratio upon stress transfer is highlighted in figure S3 of the supplementary information. This shows that a 4 μm long and 20 nm thick (aspect ratio, $s \sim 200$) BNNS has a lower Raman band shift rate than a thicker (54 nm) BNNS for which $s > 350$.

For a well-bonded 2D BNNS/polymer interface, the interfacial shear stress τ_i can be given by [40]:

$$\tau_i = nE_{\mathrm{BNNS}}\varepsilon_{\mathrm{m}}\frac{\sinh(\mathrm{ns}\frac{x}{l})}{\cosh(\mathrm{ns}/2)}. \tag{6}$$

The Young's modulus of a 17 nm thick hBN nanosheet without a top coating can be calculated using equation (2). It is found that the effective modulus of BNNSs drops from 0.87 TPa (modulus of 1L BNNS [21]) to ∼0.60 TPa when the thickness increases to 17 nm (∼50 layers). Hence the maximum value of τ_i at the edges of the 11 μm long hBN nanosheet for $ns = 10$ is calculated to be 4.7 MPa increasing to 9.4 MPa when ε_{m} is 0.05% and 0.1%, respectively. In the case of a graphene monolayer a maximum value of τ_i at 0.4% applied strain was found to be only ∼2.3 MPa [40], confirming the better stress transfer for the hBN nanosheet on the polymer substrate.

When ε_{m} is increased up to 0.15% (figure 3(h)), an approximate linear strain variation develops from the edges to the centre of the flake, up to ∼3.5 μm from the edges. It is found that shear-lag theory can no longer be used to fit the strain variation at both edges of the flake, but it still can be fitted in the centre of the flake (red dashed line), where the strain in the flake keeps almost constant at around 0.15%. This situation is analogous to the partially-debonded situation in the single fibre pull-out test [51], where interfacial failure starts at the edges of the reinforcement and propagates gradually to the centre of the fibre. In our case, it appears that the BNNS/polymer interface has started to fail at the edges of the nanosheet but continuous interfacial debonding has not reached the centre of the flake at this stage. Stress is transferred by interfacial friction [52] along the failed interface and the value of τ_i in this region can be determined from the slope of the linear fit (blue dashed line) in figure 3(h) using the force balance equation [40]:

$$\frac{\mathrm{d}\varepsilon_{\mathrm{BNNS}}}{\mathrm{d}x} = -\frac{\tau_i}{E_{\mathrm{BNNS}}t}. \tag{7}$$

which gives a value of 4.3 MPa of τ_i at edges of the flake.

When the strain is increased further to 0.3%, it is found that the BNNS/polymer interface has completely failed as shown in figure 3(i). In this case the strain linearly increases from the edges to the centre of the flake up to only ∼0.15% strain (much smaller than ε_{m}) and dips in the middle of the flake. This suggests that the interfacial debonding has reached the centre of the flake and stress transfer throughout the nanosheet is taking place through interfacial friction. In this case, the value of τ_i for the failed interface is estimated to be 3.8 MPa. This can again be contrasted with the behaviour of a graphene monolayer [40] where a value τ_i of only 0.3–0.8 MPa was determined for a failed interface at 0.6% applied strain confirming the better stress transfer for the BNNSs.

4. Conclusions

Stress transfer both between the individual layers within exfoliated hBN nanosheets and between a hBN nanosheet and a polymer substrate has been followed through the use of Raman spectroscopy. Overall, it has been demonstrated that the efficiency of stress transfer both between the individual hBN layers in the nanosheets and between the nanosheets and the substrate is better for BNNSs than for mono- or multi-layer graphene. The efficiency of interlayer stress transfer is 99% for hBN nanosheets compared with around 70% for multilayer graphene. The critical aspect ratio for stress transfer to the substrate is only ∼350 for BNNSs compared with >10^4 for monolayer graphene implying that better stress transfer to the substrate can be achieved with hBN nanosheets. The implication of this study is that BNNSs should also give rise to better reinforcement in nanocomposites than exfoliated graphene nanosheets as long as the BNNS/polymer interface remains intact. Also, it is less important to achieve a high degree of exfoliation to very thin nanosheets, when using hBN in nanocomposites, than in the case of graphite and graphene.

Data availability statement

All data that support the findings of this study are included within the article (and any supplementary files).

ORCID iDs

Zheling Li ● https://orcid.org/0000-0001-8412-0234

Alex J Marsden ⓘ https://orcid.org/0000-0002-3017-1754

Mark A Bissett ⓘ https://orcid.org/0000-0002-8908-7960

Robert J Young ⓘ https://orcid.org/0000-0001-6073-9489

References

[1] Novoselov K S 2004 Electric field effect in atomically thin carbon films *Science* **306** 666–9

[2] Gupta A, Sakthivel T and Seal S 2015 Recent development in 2D materials beyond graphene *Prog. Mater. Sci.* **73** 44–126

[3] Weng Q, Li G, Feng X, Nielsch K, Golberg D and Schmidt O G 2018 Electronic and optical properties of 2D materials constructed from light atoms *Adv. Mater.* **30** e1801600

[4] Novoselov K S, Geim A K, Morozov S, Jiang D, Katsnelson M I, Grigorieva I, Dubonos S and Firsov A A 2005 Two-dimensional gas of massless Dirac fermions in graphene *Nature* **438** 197–200

[5] Li L H, Cervenka J, Watanabe K, Taniguchi T and Chen Y 2014 Strong oxidation resistance of atomically thin boron nitride nanosheets *ACS Nano* **8** 1457–62

[6] Paine R T and Narula C K 1990 Synthetic routes to boron nitride *Chem. Rev.* **90** 73–91

[7] Weng Q, Wang X, Wang X, Bando Y and Golberg D 2016 Functionalized hexagonal boron nitride nanomaterials: emerging properties and applications *Chem. Soc. Rev.* **45** 3989–4012

[8] Cassabois G, Valvin P and Gil B 2016 Hexagonal boron nitride is an indirect bandgap semiconductor *Nat. Photon.* **10** 262

[9] Jiang X-F, Weng Q, Wang X-B, Li X, Zhang J, Golberg D and Bando Y 2015 Recent progress on fabrications and applications of boron nitride nanomaterials: a review *J. Mater. Sci. Technol.* **31** 589–98

[10] Meng W, Huang Y, Fu Y, Wang Z and Zhi C 2014 Polymer composites of boron nitride nanotubes and nanosheets *J. Mater. Chem. C* **2** 10049–61

[11] Yin J, Li J, Hang Y, Yu J, Tai G, Li X, Zhang Z and Guo W 2016 Boron nitride nanostructures: fabrication, functionalization and applications *Small* **12** 2942–68

[12] Xie B-H, Huang X and Zhang G-J 2013 High thermal conductive polyvinyl alcohol composites with hexagonal boron nitride microplatelets as fillers *Compos. Sci. Technol.* **85** 98–103

[13] Wu Y *et al* 2017 BN nanosheet/polymer films with highly anisotropic thermal conductivity for thermal management applications *ACS Appl. Mater. Interfaces* **9** 43163–70

[14] Kuang Z, Chen Y, Lu Y, Liu L, Hu S, Wen S, Mao Y and Zhang L 2015 Fabrication of highly oriented hexagonal boron nitride nanosheet/elastomer nanocomposites with high thermal conductivity *Small* **11** 1655–9

[15] Chen J, Huang X, Sun B and Jiang P 2019 Highly thermally conductive yet electrically insulating polymer/boron nitride nanosheets nanocomposite films for improved thermal management capability *ACS Nano* **13** 337–45

[16] Wu K, Wang J, Liu D, Lei C, Liu D, Lei W and Fu Q 2020 Highly thermoconductive, thermostable, and super-flexible film by engineering 1D rigid rod-like aramid nanofiber/2D boron nitride nanosheets *Adv. Mater.* **32** 1906939

[17] Zhi C, Bando Y, Tang C, Kuwahara H and Golberg D 2009 Large-scale fabrication of boron nitride nanosheets and their utilization in polymeric composites with improved thermal and mechanical properties *Adv. Mater.* **21** 2889–93

[18] Khan U, May P, O'Neill A, Bell A P, Boussac E, Martin A, Semple J and Coleman J N 2013 Polymer reinforcement using liquid-exfoliated boron nitride nanosheets *Nanoscale* **5** 581–7

[19] Wang X, Zhi C, Li L, Zeng H, Li C, Mitome M, Golberg D and Bando Y 2011 'Chemical blowing' thin-walled bubbles: high-throughput fabrication of large-area, few-layered BN and C_x-BN nanosheets *Adv. Mater.* **23** 4072–6

[20] Lee D, Lee B, Park K H, Ryu H J, Jeon S and Hong S H 2015 Scalable exfoliation process for highly soluble boron nitride nanoplatelets by hydroxide-assisted ball milling *Nano Lett.* **15** 1238–44

[21] Falin A *et al* 2017 Mechanical properties of atomically thin boron nitride and the role of interlayer interactions *Nat. Commun.* **8** 15815

[22] Song L, Ci L, Lu H, Sorokin P B, Jin C, Ni J, Kvashnin A G, Kvashnin D G, Lou J and Yakobson B I 2010 Large scale growth and characterization of atomic hexagonal boron nitride layers *Nano Lett.* **10** 3209–15

[23] Bosak A, Serrano J, Krisch M, Watanabe K, Taniguchi T and Kanda H 2006 Elasticity of hexagonal boron nitride: inelastic x-ray scattering measurements *Phys. Rev.* B **73** 041402

[24] Peng Q, Ji W and De S 2012 Mechanical properties of the hexagonal boron nitride monolayer: *ab initio* study *Comput. Mater. Sci.* **56** 11–7

[25] Wu J, Wang B, Wei Y, Yang R and Dresselhaus M 2013 Mechanics and mechanically tunable band gap in single-layer hexagonal boron-nitride *Mater. Res. Lett.* **1** 200–6

[26] Zhao S and Xue J 2013 Mechanical properties of hybrid graphene and hexagonal boron nitride sheets as revealed by molecular dynamic simulations *J. Phys. D: Appl. Phys.* **46** 135303

[27] Lee C, Wei X, Kysar J W and Hone J 2008 Measurement of the elastic properties and intrinsic strength of monolayer graphene *Science* **321** 385–8

[28] Ding N, Wu C M L and Li H 2014 The effect of grain boundaries on the mechanical properties and failure behavior of hexagonal boron nitride sheets *Phys. Chem. Chem. Phys.* **16** 23716–22

[29] Mortazavi B and Cuniberti G 2014 Mechanical properties of polycrystalline boron-nitride nanosheets *RSC Adv.* **4** 19137–43

[30] Kim S M *et al* 2015 Synthesis of large-area multilayer hexagonal boron nitride for high material performance *Nat. Commun.* **6** 8662

[31] Marom N, Bernstein J, Garel J, Tkatchenko A, Joselevich E, Kronik L and Hod O 2010 Stacking and registry effects in layered materials: the case of hexagonal boron nitride *Phys. Rev. Lett.* **105** 046801

[32] Gao W and Tkatchenko A 2015 Sliding mechanisms in multilayered hexagonal boron nitride and graphene: the effects of directionality, thickness, and sliding constraints *Phys. Rev. Lett.* **114** 096101

[33] Pakdel A, Bando Y and Golberg D 2014 Nano boron nitride flatland *Chem. Soc. Rev.* **43** 934–59

[34] Papageorgiou D G, Li Z, Liu M, Kinloch I A and Young R J 2020 Mechanisms of mechanical reinforcement by graphene and carbon nanotubes in polymer nanocomposites *Nanoscale* **12** 2228–67

[35] Li Z, Wang R, Young R J, Deng L, Yang F, Hao L, Jiao W and Liu W 2013 Control of the functionality of graphene oxide for its application in epoxy nanocomposites *Polymer* **54** 6437–46

[36] Li Z, Young R J, Wang R, Yang F, Hao L, Jiao W and Liu W 2013 The role of functional groups on graphene oxide in epoxy nanocomposites *Polymer* **54** 5821–9

[37] Li Z, Young R J, Wilson N R, Kinloch I A, Vallés C and Li Z 2016 Effect of the orientation of graphene-based nanoplatelets upon the Young's modulus of nanocomposites *Compos. Sci. Technol.* **123** 125–33

[38] Li Z, Young R J, Kinloch I A, Wilson N R, Marsden A J and Raju A P A 2015 Quantitative determination of the spatial orientation of graphene by polarized Raman spectroscopy *Carbon* **88** 215–24

[39] Li Z, Young R J and Kinloch I A 2013 Interfacial stress transfer in graphene oxide nanocomposites *ACS Appl. Mater. Interfaces* **5** 456–63

[40] Gong L, Kinloch I A, Young R J, Riaz I, Jalil R and Novoselov K S 2010 Interfacial stress transfer in a graphene monolayer nanocomposite *Adv. Mater.* **22** 2694–7

[41] Gong L, Young R J, Kinloch I A, Riaz I, Jalil R and Novoselov K S 2012 Optimizing the reinforcement of polymer-based nanocomposites by graphene *ACS Nano* **6** 2086–95

[42] Cai Q, Scullion D, Falin A, Watanabe K, Taniguchi T, Chen Y, Santos E J and Li L H 2017 Raman signature and phonon dispersion of atomically thin boron nitride *Nanoscale* **9** 3059–67

[43] Androulidakis C, Koukaras E N, Poss M, Papagelis K, Galiotis C and Tawfick S 2018 Strained hexagonal boron nitride: phonon shift and Grüneisen parameter *Phys. Rev. B* **97** 241414

[44] Novoselov K S, Jiang D, Schedin F, Booth T J, Khotkevich V V, Morozov S V and Geim A K 2005 Two-dimensional atomic crystals *Proc. Natl Acad. Sci. USA* **102** 10451–3

[45] Ferrari A C, Meyer J, Scardaci V, Casiraghi C, Lazzeri M, Mauri F, Piscanec S, Jiang D, Novoselov K and Roth S 2006 Raman spectrum of graphene and graphene layers *Phys. Rev. Lett.* **97** 187401

[46] Wang W, Li Z, Prestat E, Hashimoto T, Guan J, Kim K S, Kingston C T, Simard B and Young R J 2019 Reinforcement of polymer-based nanocomposites by thermally conductive and electrically insulating boron nitride nanotubes *ACS Appl. Nano Mater.* **3** 364–74

[47] Golla D, Chattrakun K, Watanabe K, Taniguchi T, LeRoy B J and Sandhu A 2013 Optical thickness determination of hexagonal boron nitride flakes *Appl. Phys. Lett.* **102** 161906

[48] Peng X, Wei Q and Copple A 2014 Strain-engineered direct-indirect band gap transition and its mechanism in two-dimensional phosphorene *Phys. Rev. B* **90** 085402

[49] Cox H 1952 The elasticity and strength of paper and other fibrous materials *Br. J. Appl. Phys.* **3** 72

[50] Nairn J A 1992 A variational mechanics analysis of the stresses around breaks in embedded fibers *Mech. Mater.* **13** 131–54

[51] Bannister D, Andrews M, Cervenka A and Young R 1995 Analysis of the single-fibre pull-out test by means of Raman spectroscopy: part II. Micromechanics of deformation for an aramid/epoxy system *Compos. Sci. Technol.* **53** 411–21

[52] Kelly A and Macmillan N 1986 *Strong Solids* (Oxford: Clarendon)